Acta Crystallographica Section D
Biological Crystallography
ISSN 0907-4449

The crystal structure reveals the molecular mechanism of bifunctional 3,4-dihydroxy-2-butanone 4-phosphate synthase/GTP cyclohydrolase II (Rv1415) from *Mycobacterium tuberculosis*

Mirage Singh,‡ Pankaj Kumar,§ Savita Yadav, Ruchi Gautam, Nidhi Sharma and Subramanian Karthikeyan*

CSIR – Institute of Microbial Technology, Council of Scientific and Industrial Research (CSIR), Sector 39-A, Chandigarh 160 036, India

‡ Current address: Department of Chemistry, Indiana University, Bloomington, IN 47405, USA
§ Current address: Department of Biophysics and Biophysical Chemistry, Howard Hughes Medical Institute, Johns Hopkins University School of Medicine, Baltimore, MD 21205, USA.

Correspondence e-mail: skarthik@imtech.res.in

Received 4 February 2013
Accepted 26 April 2013

PDB Reference: DHBPS/GCHII, 4i14

The enzymes 3,4-dihydroxy-2-butanone 4-phosphate synthase (DHBPS) and GTP cyclohydrolase II (GCHII) catalyze the initial steps of both branches of the bacterial riboflavin-biosynthesis pathway. The structures and molecular mechanisms of DHBPS and GCHII as separate polypeptides are known; however, their organization and molecular mechanism as a bifunctional enzyme are unknown to date. Here, the crystal structure of an essential bifunctional DHBPS/GCHII enzyme from *Mycobacterium tuberculosis* (*Mtb*-ribA2) is reported at 3.0 Å resolution. The crystal structure revealed two conformationally different molecules of *Mtb*-ribA2 in the asymmetric unit that form a dimer *via* their GCHII domains. Interestingly, analysis of the crystal packing revealed a long 'helical-like oligomer' formed by DHBPS and GCHII functional homodimers, thus generating an 'open-ended' unit-cell lattice. However, size-exclusion chromatography studies suggest that *Mtb*-ribA2 exists as a dimer in solution. To understand the discrepancy between the oligomerization observed in solution and in the crystal structure, the DHBPS (*Mtb*-DHBPS) and GCHII (*Mtb*-GCHII) domains of *Mtb*-ribA2 have been cloned, expressed and purified as His-tagged proteins. Size-exclusion chromatography studies indicated that *Mtb*-GCHII is a dimer while *Mtb*-DHBPS exists as a monomer in solution. Moreover, kinetic studies revealed that the GCHII activities of *Mtb*-ribA2 and *Mtb*-GCHII are similar, while the DHBPS activity of *Mtb*-ribA2 is much higher than that of *Mtb*-DHBPS alone. Taken together, the results strongly suggest that *Mtb*-ribA2 exists as a dimer formed through its GCHII domains and requires full-length *Mtb*-ribA2 for optimal DHBPS activity.

1. Introduction

Tuberculosis (TB), an airborne infectious bacterial disease, claims millions of life every year across the globe. The indiscriminate use of antibiotics in the past decade has led to the emergence of new strains of *Mycobacterium tuberculosis* (*Mtb*) that show multiple drug resistance. As a consequence, the mortality rate of TB patients has increased considerably (Russell *et al.*, 2010; World Health Organization, 2012). Thus, there is an urgent need to identify new drug targets and to develop new drugs against the drug-resistant *Mtb* pathogen. Recently, it has been shown that the riboflavin-biosynthesis pathway is essential for pathogens including *Mtb* but is absent in humans (Fassbinder *et al.*, 2000; Cole *et al.*, 2001; Gerdes *et al.*, 2001; Sassetti *et al.*, 2003; Long *et al.*, 2010; Griffin *et al.*, 2011). Therefore, the enzymes involved in riboflavin biosynthesis are considered to be potential antibacterial drug targets.

In bacteria, one branch of the riboflavin-biosynthesis pathway starts with DHBPS, which catalyzes the conversion of ribulose 5-phosphate (Ru5P) to 3,4-dihydroxy-2-butanone 4-phosphate (DHBP) and formate (Fig. 1*a*; Volk & Bacher, 1990, 1991; Richter *et al.*, 1992). In another branch, GCHII catalyzes the conversion of GTP (guanosine 5′-triphosphate) to 2,5-diamino-6-ribosylamino-4(3*H*)-pyrimidinone 5′-phosphate (DARP) and formate (Fig. 1*b*; Foor & Brown, 1975, 1980; Richter *et al.*, 1993). A bifunctional pyrimidine deaminase/reductase and a hitherto unknown phosphatase catalyze the formation of 4-ribitylamino-5-amino-2,6-dihydroxypyrimidine (RAADP) by sequential deamination, side-chain reduction and dephosphorylation of DARP (Burrows & Brown, 1978; Richter *et al.*, 1997; Bacher *et al.*, 1997). The condensation of RAADP with DHBP to form 6,7-dimethyl-8-ribityllumazine (DMRL) is catalyzed by lumazine synthase (Kis & Bacher, 1995; Kis *et al.*, 1995). The riboflavin synthase catalyzes the formation of one molecule of riboflavin and one molecule of RAADP using two molecules of DMRL by a dismutation reaction (Plaut, 1960, 1963; Plaut *et al.*, 1970; Fischer & Bacher, 2008). Finally, the bifunctional riboflavin kinase/FAD synthetase catalyzes the formation of flavin mononucleotide (FMN) and flavin adenine dinucleotide (FAD) by phosphorylation followed by adenylation of riboflavin (Bacher, 1991).

Biochemical and structural studies of DHBPS encoded as a separate polypeptide show that the enzyme forms a homodimer, as reported in *Escherichia coli* (Liao *et al.*, 2001; Kelly *et al.*, 2001), *Magnaporthe grisea* (Liao *et al.*, 2002), *Methanococcus jannaschii* (Steinbacher *et al.*, 2003), *Candida albicans* (Echt *et al.*, 2004) and *Salmonella typhimurium* (Kumar *et al.*, 2010). The overall structures of the DHBPS enzymes from different species are similar and they exist as dimers. Each monomer of DHBPS shows an $\alpha+\beta$ fold consisting of eight central β-strands connected together by helices and loops. The crystal structures of complexes with D-ribulose 5-phosphate (Ru5P) substrate and divalent metal ions revealed the catalytic site of the DHBPS enzyme (Liao *et al.*, 2002; Steinbacher *et al.*, 2003; Kumar *et al.*, 2010). The active site at the dimeric interface of DHBPS is formed by residues from both of the monomers. These studies also revealed that the active site of each monomer is essentially formed by two surface loops, one of which is termed the acidic active-site loop (loop1) and the other of which is termed the tyrosine loop (loop2). The acidic active-site loop undergoes a conformational change from an open or disordered conformation to a closed conformation upon binding of Ru5P and/or divalent metal ions (Liao *et al.*, 2002; Steinbacher *et al.*, 2003; Echt *et al.*, 2004; Kumar *et al.*, 2010). The metal ions are essential for catalytic activity as they bridge the residues of the acidic active-site loop and substrate, and play a role in stabilization of the substrate (Steinbacher *et al.*, 2003; Echt *et al.*, 2004; Kumar *et al.*, 2010). The tyrosine loop (loop2), on the other hand, contributes to active-site access (Steinbacher *et al.*, 2003). In addition, another surface loop (loop3) has been identified in the DHBPS domain of *Mtb*-ribA2 and shown to play a role in its dimerization. Loop3 undergoes a coil-to-helix transition at low pH, resulting in the formation of an inactive monomer (Singh *et al.*, 2011). A proposed catalytic mechanism for DHBPS suggests that the conversion of Ru5P to DHBP in the presence of divalent metal ions involves a number of catalytic steps such as enolization, ketonization, dehydration, skeleton rearrangement and formate elimination (Volk & Bacher, 1990, 1991).

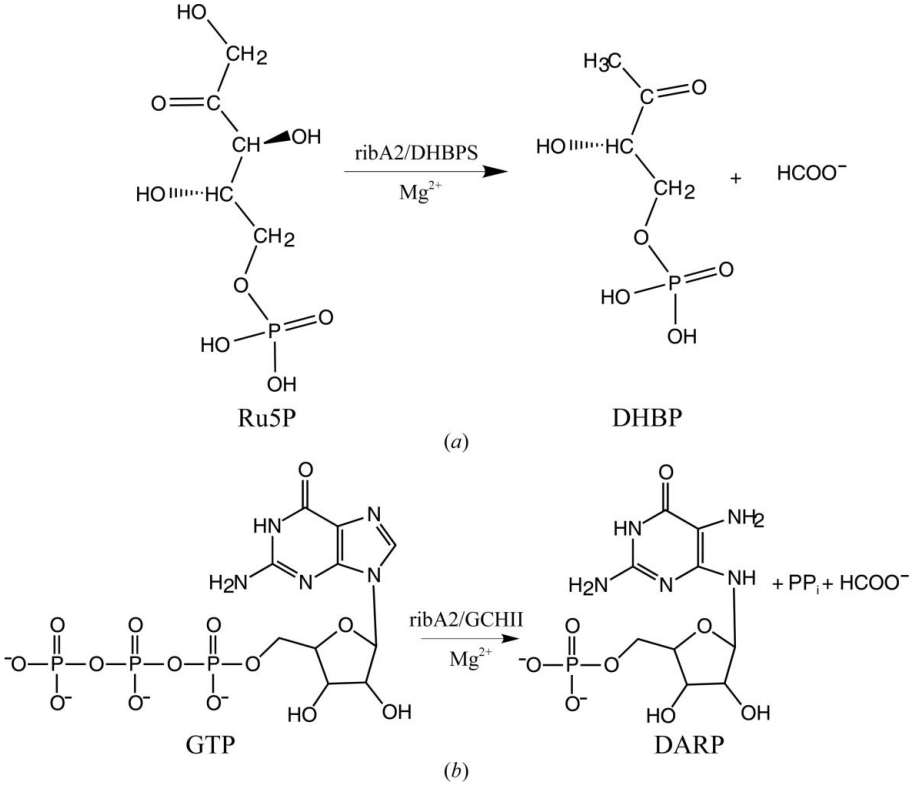

Figure 1
Reactions catalyzed by bifunctional *Mtb*-ribA2. (*a*) Reaction catalyzed by the N-terminal DHBPS domain. (*b*) Reaction catalyzed by the C-terminal GCHII domain.

The structural and biochemical characterization of GCHII from *E. coli* revealed differences from GTP cyclohydrolase I (GCHI) (Foor & Brown, 1975). The only available crystal structure of GCHII from *E. coli* shows that it has an α/β fold with an intrinsically bound zinc ion that is essential for imidazole-ring opening of GTP and the release of formate (Kaiser *et al.*, 2002; Ren *et al.*, 2005). The bound zinc ion coordinates to three cysteine residues and activates a water molecule to help in opening the imidazole ring and releasing the formate (Ren *et al.*, 2005). The crystal structure of *E. coli* GCHII in complex with its substrate analogue

GMPCPP {guanosine-5′-[(α,β)-methyleno]triphosphate} reveals the active-site residues that are involved in catalysis (Ren *et al.*, 2005). In addition, a new function has been identified in *Streptomyces coelicolor* GCHII, in which a natural single-point mutation of a catalytic tyrosine residue to methionine converts GTP to 2-amino-5-formylamino-6-ribosylamino-4-pyrimidinone 5′-phosphate instead of DARP (Spoonamore *et al.*, 2006; Spoonamore & Bandarian, 2008).

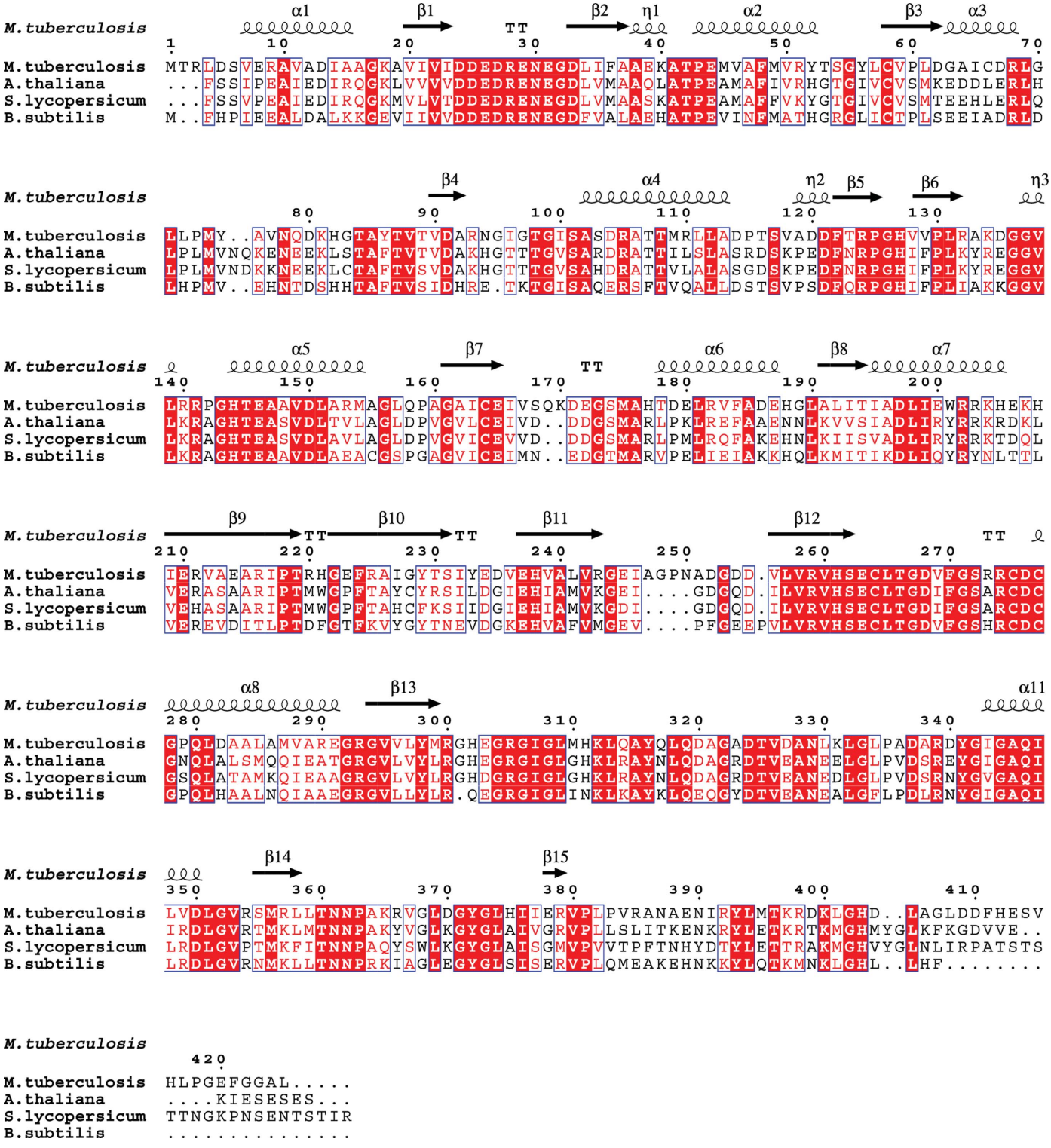

Figure 2
Multiple sequence alignment of *Mtb*-ribA2 with other reported bifunctional DHBPS/GCHII enzymes. Conserved residues are shown on a solid red background, while similar residues are shown in red. Secondary structures of *Mtb*-ribA2 are shown above the aligned sequences. The figure was generated using *MAFFT* (Katoh & Toh, 2008) and the *ESPript* (Gouet *et al.*, 1999) web server (http://espript.ibcp.fr).

The existence of a bifunctional DHBPS/GCHII enzyme has been reported in *Bacillus subtilis* (Richter *et al.*, 1993) and *S. coelicolor* (Spoonamore *et al.*, 2006), and was subsequently characterized in *Arabidopsis thaliana* and *Solanum lycopersicum* (tomato; Herz *et al.*, 2000). In addition, based on amino-acid sequence relationships, it is also predicted to be present in several species including *Rhodococcus*, *Thermotoga maritima etc*. However, in *Helicobacter pylori* the *ribBA* gene carrying both the DHBPS and GCHII domains shows only DHBPS activity and not GCHII activity (Fassbinder *et al.*, 2000). Analysis of the amino-acid sequences using *MATGAT* (Campanella *et al.*, 2003) shows about 40–65% identity among the reported species (Fig. 2). Based on sequence similarity, it has been shown that the DHBPS and GCHII domains are present at the N- and C-termini, respectively, of the bifunctional enzyme (Richter *et al.*, 1997; Herz *et al.*, 2000; Singh *et al.*, 2011). However, how these domains are assembled as a three-dimensional structure and their molecular mechanism is unknown to date. Here, we report the first crystal structure of the essential (Griffin *et al.*, 2011) bifunctional DHBPS/GCHII enzyme from *Mtb* at 3.0 Å resolution.

2. Materials and methods

2.1. Cloning, expression and purification of *Mtb*-ribA2, *Mtb*-ribA and *Mtb*-ribB

RibA2 shows 100% amino-acid sequence identity between virulent *Mtb* (strain H37Rv) and the attenuated strain H37Ra. Therefore, the *ribA2* (Rv1415) gene coding for the bifunctional DHBPS and GCHII enzyme (residues 1–425) was amplified from *Mtb* strain H37Ra genomic DNA by polymerase chain reaction (PCR) using designed forward (5′-TATTACACT**CATATG**ACGAGGTTGGACTCC-3′) and reverse (5′-TTATACATT**CTCGAG**TCACAAGGCACCGCC-3′) primers incorporating *Nde*I and *Xho*I restriction sites (bold), respectively (IDT, USA). The amplified PCR product was gel-purified using a commercial kit (Qiagen, Germany) and digested with *Nde*I and *Xho*I restriction enzymes (New England Biolabs, USA) at 310 K for 5 h. The digested PCR product after purification was ligated with pET28c vector (Novagen Inc., USA) that had previously been digested with the same set of restriction enzymes. The integration of the *Mtb-ribA2* gene in the pET28c vector was verified by DNA sequencing. The resulting clone was named pET28c-*mribA2*. PCR amplification of the DHBPS domain of *Mtb-ribA2* (residues 1–206) was carried out using forward (5′-TATTACACT**CATATG**ACGAGGTTGGACTCC-3′) and reverse (5′-TATTACATT**CTCGAG**TCACTCATGCTTGCGCCG-3′) primers using pET28c-*mribA2* as template. Similarly, PCR amplification of the GCHII domain of *Mtb-ribA2* (residues 207–425) was performed using forward (5′-TTATACATT-**CATATG**GAGAAGCACATTGAG-3′) and reverse (5′-TTATACATT**CTCGAG**TCACAAGGCACCGCC-3′) primers. The amplified individual DHBPS and GCHII domains of *Mtb-ribA2* were ligated into pET28c vector and verified by DNA sequencing. The resulting plasmids for the DHBPS and GCHII domains of *Mtb-ribA2* were named pET28c-*mDHBPS* and pET28c-*mGCHII*, respectively.

For the expression of *Mtb*-ribA2, the pET28c-*mribA2* plasmid was transformed into *E. coli* BL21 (DE3) strain using standard protocols. A single colony from a Luria–Bertani (LB) agar–kanamycin (30 µg ml^{-1}) plate was used to inoculate 10 ml LB medium supplemented with kanamycin (30 µg ml^{-1}) and allowed to grow at 310 K overnight. A secondary culture with 1 l LB–kanamycin medium was inoculated with 1%(*v*/*v*) of the overnight-grown seed culture. The secondary culture was further grown at 310 K until the optical density at 600 nm reached a value of 0.6, after which the temperature was reduced to 298 K. At 298 K, the culture was induced with 0.5 m*M* isopropyl β-D-1-thiogalactopyranoside (IPTG) and incubated for a further 16 h at 298 K for protein expression. The cells were harvested by centrifuging the culture at 6000*g* for 15 min at 277 K. After discarding the supernatant, the cell pellet was resuspended in lysis buffer composed of 50 m*M* Tris–HCl pH 8.0, 150 m*M* NaCl, 1 m*M* PMSF, protease-inhibitor cocktail (Roche, USA) and 1 mg ml^{-1} lysozyme. The resuspended cells were lysed either by passing twice through a French press (SLM-AMINCO; Spectronic Instruments Inc., USA) at 10.3 MPa or by sonication (Sonics, USA) for 30 min with pulses of 30 s on and 30 s off (20% amplitude). The lysed cells were centrifuged at 15 000*g* for 30 min at 277 K to remove cell debris and the supernatant was passed through an Ni–NTA column (Qiagen, Germany) pre-equilibrated with equilibration buffer (50 m*M* Tris–HCl pH 8.0, 150 m*M* NaCl, 10 m*M* imidazole). After passing the supernatant through the Ni–NTA column, the column was washed with ten column volumes of wash buffer (50 m*M* Tris–HCl pH 8.0, 150 m*M* NaCl, 40 m*M* imidazole) to remove any nonspecifically bound proteins. Finally, the *Mtb*-ribA2 was eluted with 50 m*M* Tris–HCl pH 8.0, 150 m*M* NaCl, 200 m*M* imidazole and dialyzed against 50 m*M* Tris–HCl pH 8.0, 150 m*M* NaCl, 1 m*M* DTT using a 10 kDa cutoff membrane (Small Wonder-Lyzer; US Patent No. 6 368 509) overnight. The dialyzed *Mtb*-ribA2 was further purified by size-exclusion chromatography using a pre-packed Sephacryl S-200 column (GE Healthcare, USA) followed by concentration using an Amicon concentrator with a 10 kDa cutoff membrane (Millipore, USA). The purity of the protein at each stage was checked by SDS–PAGE (Laemmli, 1970) and the concentration was estimated by the Bradford method (Bradford, 1976). Similarly, *Mtb*-DHBPS was expressed using 0.25 m*M* IPTG and incubated for a further 4 h at 310 K (Singh *et al.*, 2011), while *Mtb*-GCHII was expressed using 0.25 m*M* IPTG and incubated at 298 K overnight. Both *Mtb*-DHBPS and *Mtb*-GCHII were purified using the same protocol as used for *Mtb*-ribA2 and were finally dialyzed against 50 m*M* Tris–HCl pH 8.0, 150 m*M* NaCl, 1 m*M* DTT.

2.2. Size-exclusion chromatography

To determine the oligomeric status of *Mtb*-ribA2, *Mtb*-DHBPS and *Mtb*-GCHII, the individual proteins were passed through a pre-packed Sephacryl S-200 size-exclusion

chromatography preparative column (GE Healthcare, USA) that had been pre-equilibrated with 50 m*M* Tris–HCl pH 8.0, 150 m*M* NaCl, 1 m*M* DTT (flow rate 0.5 ml min^{-1}). Different molecular-weight protein standards were run on the Sephacryl S-200 column equilibrated with the same buffer to establish an elution volume–molecular weight relationship. The proteins used as standards were aldolase (158 kDa), conalbumin (75 kDa), ovalbumin (43 kDa), carbonic anhydrase (29 kDa) and ribonuclease A (13.7 kDa) (GE Healthcare, USA).

2.3. Enzyme activity of *Mtb*-ribA2

The DHBPS activities of *Mtb*-ribA2 and *Mtb*-DHBPS were measured by a colorimetric method as described by Picollelli *et al.* (2000). Briefly, the enzyme was mixed with 50 m*M* Tris–HCl pH 8.0, 150 m*M* NaCl, 10 m*M* $MgCl_2$, D-ribose 5-phosphate and 0.25 units of phosphoriboisomerase (Sigma, USA) in a 125 µl reaction volume in a 96-well ELISA plate and incubated at 310 K for 30 min. The colour was developed by the addition of 100 µl saturated creatine solution followed by 50 µl α-naphthol (35 mg ml^{-1} in 1.0 *N* NaOH) to the reaction mixture, and the absorbance at 525 nm was measured after 30 min using an ELISA plate reader (BioTek PowerWave XS, USA). The values were compared with a standard plot that was established with 0–50 nmol 2,3-butadione to calculate the amount of product (DHBP) formation. The K_m and V_{max} values were determined by varying the substrate concentration from 40 µ*M* to 3.5 m*M* using 25 µg *Mtb*-ribA2 or *Mtb*-DHBPS. At least three readings were taken for each concentration of substrate and nonlinear curve fitting was used to calculate the kinetic parameters.

The GCHII activities of *Mtb*-ribA2 and *Mtb*-GCHII were measured as described by Lehmann *et al.* (2009). Briefly, the enzyme was mixed with 50 m*M* Tris–HCl pH 8.0, 100 m*M* NaCl, 2 m*M* DTT and 10 m*M* $MgCl_2$ in a total reaction volume of 200 µl. Reaction was initiated by the addition of a known concentration of GTP followed by incubation at 310 K for 20 min. To monitor the formation of DARP, the absorbance was measured at 310 nm using a spectrophotometer. The reaction rate was calculated using an extinction coefficient of 7.43 mM^{-1} cm^{-1} for DARP (Lehmann *et al.*, 2009). The experiments were carried out in a 96-well plate and the absorbance was recorded using an ELISA plate reader (BioTek PowerWave XS, USA). The kinetic parameters were determined by varying the concentration of substrate using 20 µg enzyme. At least three readings were taken for each concentration of substrate and nonlinear curve fitting was used to calculate the kinetic parameters.

2.4. Crystallization of *Mtb*-ribA2

The purified *Mtb*-ribA2 (using the pET28c-*mribA2* clone) was concentrated to 20–25 mg ml^{-1} using Amicon centrifugal concentrators with a 10 kDa cutoff membrane (Millipore, USA). The concentrated protein in 20 m*M* Tris–HCl pH 8.0, 150 m*M* NaCl, 1 m*M* DTT was used for crystallization by the vapour-diffusion method in 96-well sitting-drop plates (MRC plates, Molecular Dimensions, UK). Initial crystallization screening was carried out using commercial kits from Qiagen (Germany) and Hampton Research (USA) by mixing 1 µl reservoir buffer and 1 µl protein solution and equilibrating against 40 µl reservoir buffer at 293 K. Small crystals appeared after 2 d when *Mtb*-ribA2 was equilibrated against 0.1 *M* Na HEPES pH 7.5, 15%(*w*/*v*) PEG 8000. The crystal size was improved to 0.4 × 0.2 × 0.2 mm by the sitting-drop method by changing the protein:buffer ratio to 2:1.5 and incubating the plate at 293 K for 2–4 d.

2.5. Data collection and processing

X-ray diffraction data were collected from the *Mtb*-ribA2 crystal using an in-house MAR345dtb imaging-plate detector (MAR Research, Germany) mounted on a rotating-anode X-ray generator (Rigaku MicroMax-007 HF) operated at 40 kV and 30 mA. The data were collected under cryogenic conditions at 100 K using an Oxford cryostream system. A single crystal was soaked in a cryoprotectant solution

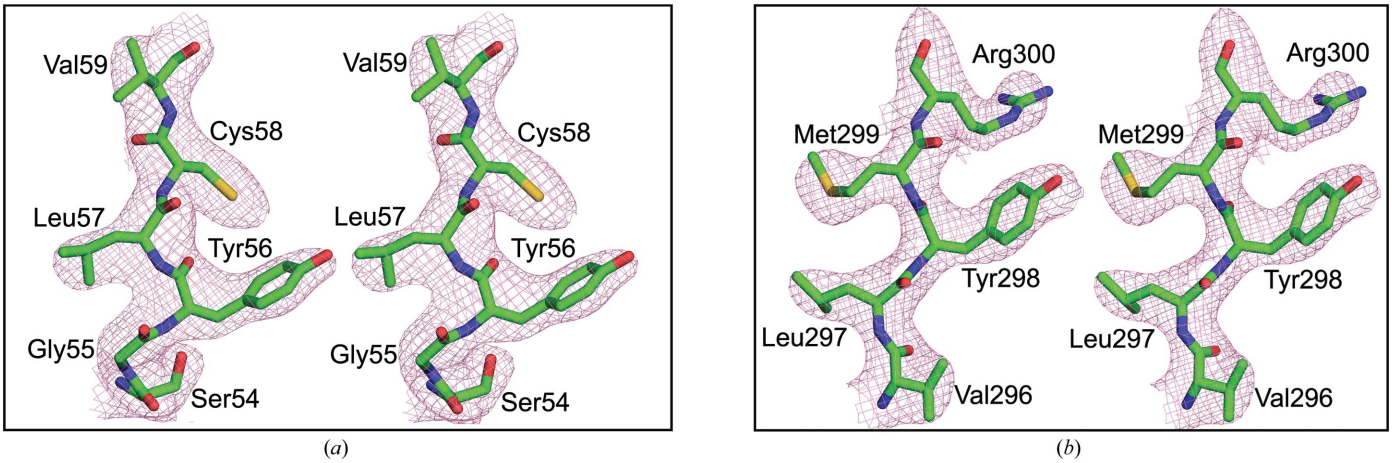

(*a*) (*b*)

Figure 3
Quality of the electron-density map for *Mtb*-ribA2. Stereoviews showing the final Fourier electron-density map ($2F_o - F_c$) contoured at the 1.0σ level (*a*) for the DHBPS domain, (*b*) for the GCHII domain

Table 1
Data-collection and processing for *Mtb*-ribA2.

Values in parentheses are for the last resolution shell.

Wavelength (Å)	1.542
No. of crystals used	1
Resolution range (Å)	20.0–3.0 (3.18–3.00)
Space group	$P2_12_12$
Unit-cell parameters (Å)	a = 168.8, b = 74.8, c = 76.4
Total No. of reflections	80480
Unique reflections	19733
Mosaicity (°)	0.1
Multiplicity	4.1 (4.0)
$\langle I/\sigma(I)\rangle$	20.8 (4.5)
Completeness (%)	98.6 (95.8)
$R_{\rm merge}$† (%)	5.8 (30.0)

† $R_{\rm merge} = \sum_{hkl}\sum_i |I_i(hkl) - \langle I(hkl)\rangle|/\sum_{hkl}\sum_i I_i(hkl)$, where $I(hkl)$ is the intensity of reflection hkl.

consisting of 20%(*v*/*v*) glycerol in the mother liquor and flash-cooled prior to data collection (Teng, 1990). The crystal-to-detector distance was kept at 300 mm and a complete data set was obtained from 206 images with 0.5° oscillation and an exposure time of 10 min per image. The diffraction intensities were integrated and scaled using the *XDS* suite of programs (Kabsch, 2010). The scaled intensities were converted to amplitudes using *TRUNCATE* (French & Wilson, 1978) as implemented in the *CCP*4 suite (Winn *et al.*, 2011). Although the experimental setup that was used for data collection limited the available resolution to 3.0 Å, the data-processing statistics suggested that the crystal might be capable of yielding somewhat higher resolution data.

2.6. Structure determination and refinement

The *Mtb*-ribA2 structure was solved by the molecular-replacement method using the *E. coli* DHBPS and GCHII structures (PDB entries 1g57 and 2bz1; Liao *et al.*, 2001; Ren *et al.*, 2005) as search models (poly-Ala) in *Phaser* (McCoy *et al.*, 2007) with default parameters through *CCP*4. During structure determination, the DHBPS dimer model was first located and fixed and GCHII was then located using the automatic search option in the *Phaser* program. *Phaser* yielded a single solution with two molecules of *Mtb*-ribA2 in the asymmetric unit. The initial model was refined as a rigid body followed by a combination of TLS (translation/libration/screw) and restrained refinement in *REFMAC*5 (Murshudov *et al.*, 2011). The TLS refinement was performed by considering the two DHBPS domains (residues *A*1–*A*208 and *B*1–*B*202) and the two GCHII domains (residues *A*209–*A*383 and *B*203–*B*383) as different TLS groups as suggested by the *TLSMD* server (Painter & Merritt, 2006). For cross-validation, a random set of 5% of the total reflections was kept aside from the refinement and used for the calculation of $R_{\rm free}$ (Brünger, 1992). The model was built manually into the electron-density map using *Coot* (Emsley *et al.*, 2010). Refinement and model building were carried out iteratively until the model was completely built and no further improvement of the model was observed.

Table 2
Structure refinement and validation for *Mtb*-ribA2.

Resolution range (Å)	19.7–3.0
Unique reflections	19733
Completeness (%)	99.0
$R_{\rm cryst}$† (%)	19.8
$R_{\rm free}$‡ (%)	26.3
R.m.s.d.s	
Bond lengths (Å)	0.006
Bond angles (°)	1.120
Ramachandran plot, residues in	
Most favoured region (%)	90.2
Additionally allowed region (%)	9.8
Mtb-ribA2 model	
No. of modelled residues	647
No. of water molecules	7
No. of sulfate ions	2
No. of zinc ions	2
Average B factors (Å^2)	
Protein atoms	61.7
Water molecules	36.8
Sulfate ions	45.4
Zinc ions	55.4
PDB code	4i14

† $R_{\rm cryst} = \sum_{hkl}\big||F_{\rm obs}| - |F_{\rm calc}|\big|/\sum_{hkl}|F_{\rm obs}|$. ‡ $R_{\rm free}$ is the cross-validation R factor computed for the test set of 5% of unique reflections.

3. Results and discussion

3.1. Crystallographic details of *Mtb*-ribA2

The *Mtb*-ribA2 crystal belonged to space group $P2_12_12$, with unit-cell parameters a = 168.76, b = 74.83, c = 76.42 Å, and an X-ray diffraction data set was collected to 3.0 Å resolution. The data-collection and processing statistics are shown in Table 1. Matrix-assisted laser desorption ionization (MALDI) studies revealed the molecular weight of *Mtb*-ribA2 to be 48 163 Da. including 2181 Da contributed by the 20 extra N-terminal amino-acid residues (N-MGSSHHHHHHSSG-LVPRGSH) from the cloning vector (pET28c-*mribA2*). However, the molecular weight estimated from the elution volume of size-exclusion chromatography studies was about 90 kDa, suggesting that *Mtb*-ribA2 exists as dimer in solution (Supplementary Fig. S1[1]). Thus, assuming the presence of two molecules of *Mtb*-ribA2 in the asymmetric unit, the calculated Matthews coefficient (Matthews, 1968; $V_{\rm M}$) and solvent content were 2.51 Å^3 Da^{-1} and 50.9%, respectively. The *Mtb*-ribA2 structure was solved by the molecular-replacement method using the structures of DHBPS and GCHII from *E. coli* (PDB entries 1g57 and 2bz1; Liao *et al.*, 2001; Ren *et al.*, 2005) as search models. The asymmetric unit contained two molecules of *Mtb*-ribA2 that form a dimer through their GCHII domains, while the DHBPS domain forms a homo-dimer with the neighbouring asymmetric unit. The overall electron density was clear and we were able to build most of the residues into the electron-density map (Fig. 3), with the exception of residues 76–84, 249–251, 301–340, 364–369 and 384–425 in chain *A*, and residues 75–85, 247–252, 301–340, 365–369 and 383–425 in chain *B*, which could not be traced in the electron-density map and thus were not included in the

[1] Supplementary material has been deposited in the IUCr electronic archive (Reference: WD5206). Services for accessing this material are described at the back of the journal.

model. During refinement, the difference Fourier map consistently showed electron density at above the 3σ level in the DHBPS and GCHII domains of *Mtb*-ribA2. In the DHBPS domain we modelled this density as a sulfate ion, as this position is always occupied by sulfate or phosphate in *Mtb*-DHBPS (Singh *et al.*, 2011). In the GCHII domain the electron density was modelled as a zinc ion. Although it is difficult to identify the Zn ion at this resolution, refinement with other potential molecules such as water, Mg^{2+} and Mn^{2+} did not show acceptable refinement parameters in terms of the difference Fourier map and temperature factor. Moreover, it has been shown that a Zn ion is essential at the catalytic site of GCHII for its activity (Kaiser *et al.*, 2002). Therefore, based on these criteria we modelled the electron density as a Zn ion in the GCHII domain. However, the zinc and sulfate ions are refined with partial occupancy. The final model of *Mtb*-ribA2 consists of 645 residues, two zinc ions, two sulfates and seven water molecules, with an *R* factor of 19.8% and an R_{free} of 26.3%. A Ramachandran plot analysis of the final model using *PROCHECK* (Laskowski *et al.*, 1993) showed that 90.2% of the residues are in the most favoured region, while 9.8% of the residues are in the additionally allowed region. The final refinement statistics are shown in Table 2.

3.2. Overall crystal structure of *Mtb*-ribA2

The overall topology of *Mtb*-ribA2 consists of two domains present at the N- and C-termini interconnected by a short linker region from residues 206 to 208. The N-terminal domain (residues 1–205) is an $\alpha+\beta$ fold with central core of eight β-strands interconnected by loops or helices and represents the DHBPS domain of *Mtb*-ribA2 (Fig. 4*a*). The C-terminal domain of *Mtb*-ribA2 (residues 209–425) shows a typical α/β fold with a central core of mainly antiparallel β-strands flanked by two α-helices and represents the GCHII domain (Fig. 4*a*). The asymmetric unit consists of two molecules of *Mtb*-ribA2 that form a dimer through their GCHII domains (Fig. 4*b*). A similarity search using the *PDBeFold* (*SSM*) server (Krissinel & Henrick, 2004) against the whole Protein Data Bank (PDB) reveals that there are no similar structures to *Mtb*-ribA2 in the existing database. However, the DHBPS and GCHII domains of *Mtb*-ribA2 are structurally similar to DHBPS and GCHII from other organisms in which they are encoded as separate polypeptides. The most similar structure to the DHBPS domain of *Mtb*-ribA2 is DHBPS from *C. albicans* (PDB entry 1tks; Echt *et al.*, 2004), with a *Z*-score of 17.2 and a root-mean-square (r.m.s.) deviation of 0.88 Å for 185 C^{α} atoms. The GCHII domain of *Mtb*-ribA2 shows similarity to the only available *E. coli* structure (PDB entry 2bz0; Ren *et al.*, 2005), with a *Z*-score of 12.8 and an r.m.s. deviation of 1.11 Å for 120 C^{α} atoms. Interestingly, superposition of the two molecules of *Mtb*-ribA2 in the asymmetric unit (Fig. 4*c*) using *LSQMAN* (Kleywegt, 1996) shows an r.m.s. deviation of 6.6 Å for 321 C^{α} atoms. However, superposition of the DHBPS domains and GCHII domains from each molecule of *Mtb*-ribA2 shows r.m.s. deviations of 0.45 Å (for 197 C^{α} atoms) and 0.73 Å (for 122 C^{α} atoms), respectively, indicating that the relative orientation of the DHBPS and GCHII

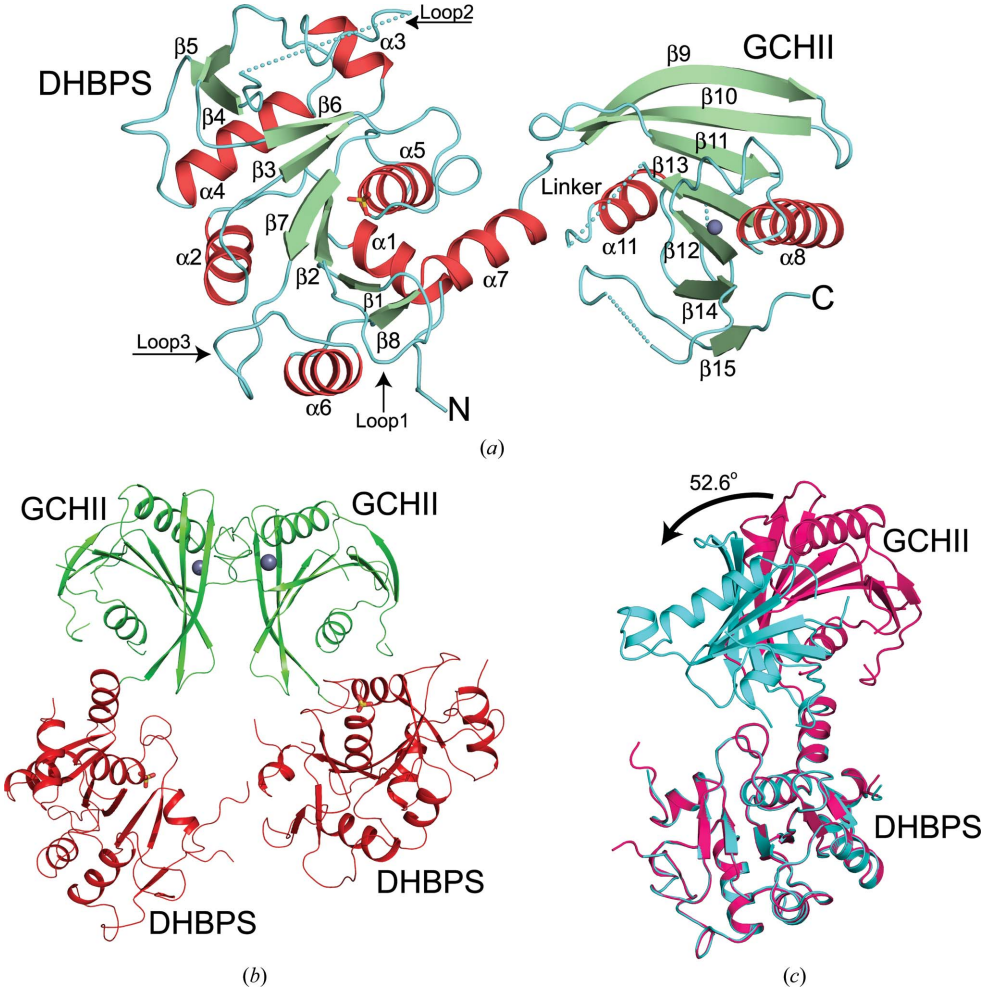

Figure 4
Crystal structure of *Mtb*-ribA2. (*a*) Overall three-dimensional structure of *Mtb*-ribA2. Secondary structures are labelled and shown in different colours. Dashed lines indicate the disordered regions in the crystal structure. (*b*) Dimer interface formed between the GCHII domains of two monomers in the asymmetric unit. Zinc ions are shown as spheres and sulfate ions are shown as sticks. (*c*) Structural superposition of two molecules of *Mtb*-ribA2 (cyan and magenta) shows the relative movement of the GCHII and DHBPS domains along the linker region as a hinge axis.

domains is different in each monomer. Further analysis of the domain movement using the *DynDom* server (Hayward & Berendsen, 1998) reveals that the relative orientation of the two molecules differs by 52.6° with a hinge axis anchored at the linker region (residues 205–209), suggesting that *Mtb*-ribA2 possesses two different conformations in the asymmetric unit (Fig. 4*c*).

3.3. DHBPS domain of *Mtb*-ribA2

The N-terminal DHBPS domain of *Mtb*-ribA2 shows an $\alpha+\beta$ fold (Fig. 4*a*) consisting of a central eight-stranded β-sheet ($\beta1$–$\beta8$) surrounded by seven helices ($\alpha1$–$\alpha7$), identical to the structure reported previously for *Mtb*-DHBPS (Singh *et al.*, 2011). The active-site loop (loop1 in Fig. 4*a*; residues 24–31) is observed in an open conformation, while the loop responsible for the proposed substrate channelling (loop2 in Fig. 4*a*; residues 75–84) is disordered owing to the absence of bound substrate (Steinbacher *et al.*, 2003; Echt *et al.*, 2004). The proposed pH-sensitive loop (loop3 in Fig. 4*a*; residues 165–177) is observed in a loop conformation as reported previously (Singh *et al.*, 2011). The functional DHBPS dimer would be formed by applying twofold crystallographic symmetry, as shown in Fig. 5. The active site is located at two topologically similar sites at the dimeric interface of two monomers, as observed in other species. A sulfate ion is bound to both of the monomers of DHBPS and occupies a similar position to the phosphate moiety of the substrate ribulose 5-phosphate (Ru5P). As previously shown, the interactions between two DHBPS monomers are mediated mostly by hydrogen-bond interactions rather than hydrophobic interactions as observed in other species (Singh *et al.*, 2011). Structural alignment of the DHBPS domain of *Mtb*-ribA2 with DHBPS from *E. coli* (Liao *et al.*, 2001), *M. grisea* (Liao *et al.*, 2002), *M. jannaschii* (Steinbacher *et al.*, 2003) and *C. albicans* (Echt *et al.*, 2004) shows r.m.s. deviations of 1.16, 0.96, 1.28 and 0.85 Å for 178, 177, 169 and 183 C^{α} atoms, respectively. Moreover, the active-site residues are conserved in all of these species, suggesting that they will all have a similar catalytic mechanism (Singh *et al.*, 2011).

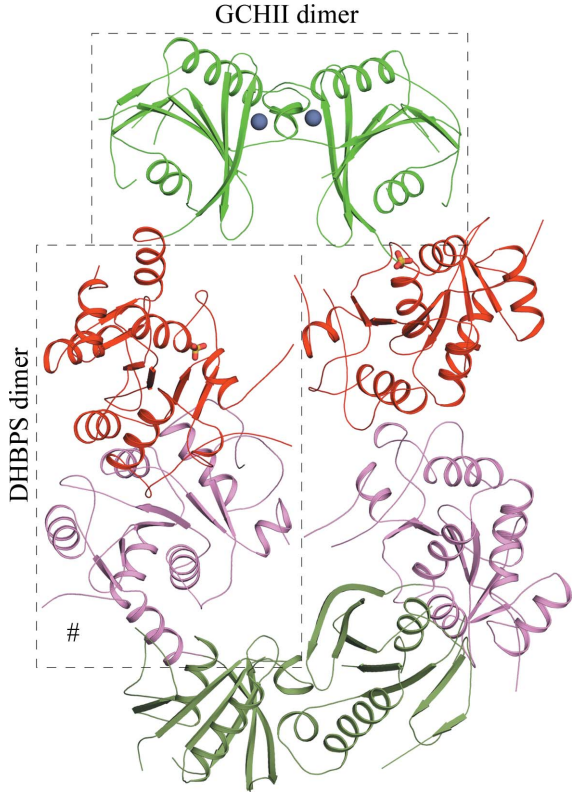

Figure 5
Arrangement of the biological dimer of GCHII and DHBPS domains. The dimer interface formed between the GCHII domains of two monomers in the same asymmetric unit and the DHBPS domain with the neighbouring asymmetric unit is indicated by '#'.

3.4. GCHII domain of *Mtb*-ribA2

The C-terminal GCHII domain of *Mtb*-ribA2 adopts an α/β fold with a central core of mainly antiparallel β-strands ($\beta9$–$\beta15$) flanked by two α-helices ($\alpha8$ and $\alpha11$), as shown in Fig. 4(*a*). Residues 300–340, 364–370 and 383–425 could not be traced in the electron-density map for both monomers and thus were not included in the final model of *Mtb*-ribA2. The difference Fourier map of *Mtb*-ribA2 consistently showed electron density at above the 3σ level (Fig. 6*a*) between $\beta12$ and $\alpha8$ surrounded by three conserved cysteine residues (Cys264, Cys275 and Cys277). This electron density was modelled as a zinc ion and was refined with partial occupancy. Although we did not add zinc ions explicitly during protein preparation or crystallization, it is likely that the zinc ion was bound intrinsically, similar to the previously reported *E. coli* GCHII structure (Ren *et al.*, 2005). In addition, a water molecule is also modelled in the electron-density map near the zinc ion as it forms a fourth coordination bond to the bound zinc ion (Fig. 6*a*). In the *E. coli* GCHII structure the zinc ion, along with a water molecule, has been proposed to play a role in ring-opening of the GTP substrate (Ren *et al.*, 2005).

E. coli GCHII forms a dimer in solution (Foor & Brown, 1975) as well in the crystal structure (Ren *et al.*, 2005). Similarly, the crystal structure of *Mtb*-ribA2 shows association of the GCHII domain as a dimer similar to that observed in *E. coli* (Fig. 6*b*). The dimeric interface of GCHII is formed by amino acids contributed from both monomers. The carbonyl O atom of Pro218 from one monomer forms a hydrogen bond to the backbone amide of Arg273 of the other monomer. The residue Arg273 is replaced by leucine in other species, while Pro218 is strictly conserved. Similarly, Arg300 NH2 forms a hydrogen bond to Glu263 OE2 and both residues are highly conserved. Moreover, most of the interactions leading to the formation of the dimeric interface are hydrophobic and are mainly provided by the residues (210–218) of $\beta9$ and the loop between $\beta9$ and $\beta10$ of one monomer and the residues (265–270) of the loop between $\beta12$ and $\alpha8$ of the other monomer. In addition, the residues (208–212) of $\beta9$ of one monomer are also reported to form hydrophobic interactions with the loop residues (313–320) present between $\beta13$ and $\alpha9$ of the other monomer in *E. coli*, but as residues 300–340 are not defined by electron density in *Mtb*-ribA2 these interactions are not

observed in the present crystal structure. Structural superposition of the GCHII domain of *Mtb*-ribA2 with GCHII of *E. coli* shows an r.m.s. deviation of 1.06 Å for 120 C^{α} atoms (Fig. 6*b*). The superposition shows that the region 301–340 which is disordered in *Mtb*-ribA2 forms an extended region consisting of two helices (α9 and α10) above the main body of the protein as observed in *E. coli* GCHII (Fig. 6*b*). Although a portion of the active-site residues in the GCHII domain are absent, we speculate that the proposed catalytic mechanism for *E. coli* GCHII will be similar in *Mtb*-ribA2 as most of the catalytic residues are conserved in both species.

3.5. *Mtb*-ribA2 exists as a dimer formed through its GCHII domain

The crystal structure of *Mtb*-ribA2 shows two molecules in the asymmetric unit forming a functional dimer through their GCHII domains. However, analysis of the crystal packing revealed that the DHBPS domain of each monomer in one asymmetric unit also forms a functional dimer with the DHBPS domain of the neighbouring asymmetric unit (Fig. 5). In fact, the crystal structure can be refined with two molecules of *Mtb*-ribA2 in the asymmetric unit forming a homodimer either through their GCHII or DHBPS domains (Figs. 7*a* and 7*b*). The spatial arrangement of *Mtb*-ribA2 molecules in this way forms a 'helical-like oligomer' composed of both DHBPS and GCHII dimers and thus generates an 'open-ended' unit-cell lattice in the crystal (Fig. 7*c*). A quaternary-structure assembly analysis using the *PISA* server (Krissinel & Henrick, 2007) indicates two stable dimers formed by GCHII domains in the same asymmetric unit and by DHBPS domains from the same and neighbouring asymmetric units with a buried surface areas of 2001 $Å^2$ (6.5% of the total accessible surface area; ASA) and 2258 $Å^2$ (7.4% of the total ASA), respectively. Interestingly, the gel-filtration experiment strongly suggested that *Mtb*-ribA2 exists as a dimer in solution (Supplementary Fig. S1). However, from the crystal structure of *Mtb*-ribA2 it is not clear whether the observed dimer in solution is formed through its GCHII or its DHBPS domain. Thus, to explore the domains involved in dimer formation of *Mtb*-ribA2 in solution, we have individually cloned, expressed and purified the DHBPS domain (*Mtb*-DHBPS) and the GCHII domain (*Mtb*-GCHII) of *Mtb*-ribA2 as His-tagged proteins. Size-exclusion chromatography studies indicate that *Mtb*-GCHII exists as a dimer, while *Mtb*-DHBPS elutes as a monomer in the buffer used for full-length *Mtb*-ribA2 (Supplementary Fig. S2*a*). Taken together, these studies strongly suggest that *Mtb*-ribA2 exists as a dimer formed through its GCHII domains, while its DHBPS domain forms a monomer in solution.

3.6. Full-length *Mtb*-ribA2 is required for optimal DHBPS activity

The existence of the DHBPS domain in *Mtb*-ribA2 as a monomer in solution is surprising because DHBPS is required to be a homodimer for activity as the catalytic active site is formed at the dimeric interface of DHBPS monomers (Liao *et al.*, 2002; Steinbacher *et al.*, 2003; Echt *et al.*, 2004; Kumar *et al.*, 2010). Thus, to understand the enzymatic activity of *Mtb*-ribA2, kinetic values for both the DHBPS and GCHII activities were calculated using steady-state kinetics. The GCHII activity of *Mtb*-ribA2 has K_m and k_{cat} values of 126.7 μM and 0.21 min^{-1}, respectively, while *Mtb*-GCHII has K_m and k_{cat} values of 150.5 μM and 0.37 min^{-1}, respectively (Table 3), indicating that no significant change is observed in the GCHII activities of either *Mtb*-ribA2 or *Mtb*-GCHII (Supplementary Figs. S3*a* and S3*b*). This is consistent with the fact that the GCHII domains of *Mtb*-ribA2 and *Mtb*-GCHII always exist as a dimer and may catalyze the formation of the product in a similar manner.

Steady-state kinetics gives K_m and k_{cat} values of 918.7 μM and 2.5 min^{-1}, respectively, for the DHBPS activity of *Mtb*-ribA2 (Supplementary Fig. S3*c*), while *Mtb*-DHBPS has very poor DHBPS activity and we were unable to calculate its kinetic parameters (Table 3). This result is very surprising because the DHBPS domains of both *Mtb*-ribA2 and

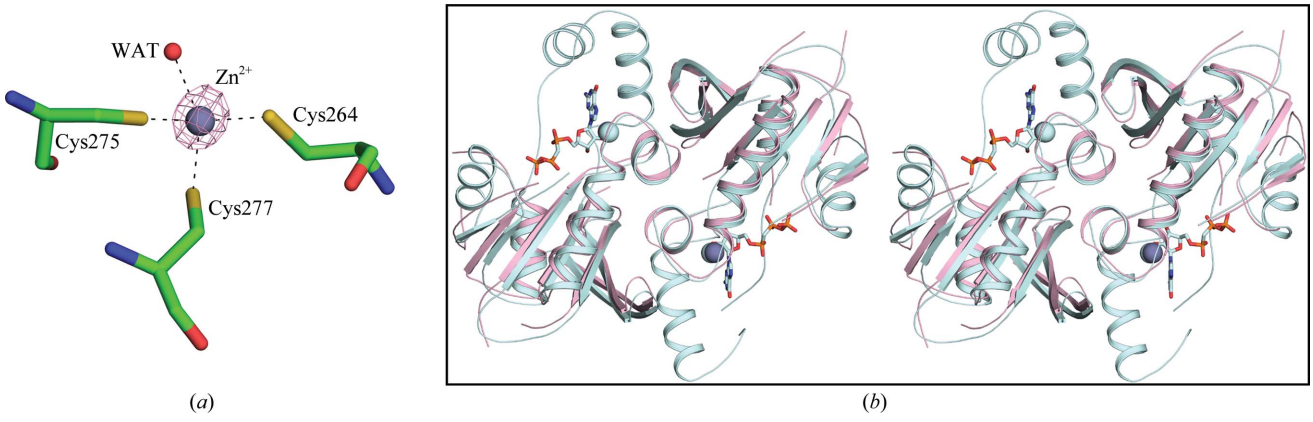

Figure 6
GCHII domain of *Mtb*-ribA2. (*a*) The coordination of the intrinsically bound zinc ion by three cysteine residues and one water molecule in the GCHII domain of *Mtb*-ribA2. The difference Fourier electron-density map ($F_o - F_c$) contoured at the 3.0σ level for the bound zinc ion is shown in magenta. (*b*) Stereoview of superposition of the GCHII domain of *Mtb*-ribA2 (magenta) on *E. coli* GCHII (cyan). The bound GTP analogue (GMPCPP) in *E. coli* GCHII is shown in stick representation, while the bound zinc ions in *Mtb*-ribA2 (violet) and *E. coli* GCHII (cyan) are shown as spheres.

Table 3
Kinetic parameters for *Mtb*-ribA2, *Mtb*-GCHII and *Mtb*-DHBPS.

N.D., not detectable at 25 µg protein concentration.

Substrate	Protein	K_m (µ*M*)	V_{max} (nmol min^{-1} mg^{-1})	k_{cat} (min^{-1})	k_{cat}/K_m (m*M*$^{-1}$ min^{-1})
GTP	*Mtb*-ribA2	126.7 ± 8.7	4.5 ± 0.1	0.2	1.4
	Mtb-GCHII	150.5 ± 11.4	9.3 ± 0.2	0.3	2.1
D-Ribulose 5-phosphate	*Mtb*-ribA2	918.7 ± 112.3	52.3 ± 3.7	2.5	2.7
	Mtb-DHBPS	N.D.	N.D.	N.D.	N.D.

Mtb-DHBPS exist as monomers in solution; however, *Mtb*-ribA2 shows DHBPS catalytic activity while *Mtb*-DHBPS shows negligible catalytic activity. To investigate whether the presence of the GHCII domain is required for DHBPS activity, we checked the activity of *Mtb*-DHBPS in the presence of *Mtb*-GCHII. However, the calculated kinetic values did not show any significant change, suggesting that the GCHII domain is not required for DHBPS activity. Although it is unclear how the DHBPS domain of *Mtb*-ribA2 can be functional as a monomer, as the active site is formed at the dimeric interface, we speculate that in the presence of substrate the DHBPS domain of *Mtb*-ribA2 may transiently form a dimer and may show catalytic activity. Moreover, we predict that the orientation of the DHBPS domain in *Mtb*-ribA2 may play a role in facilitating transient dimer formation as this orientation may be lost in *Mtb*-DHBPS alone. These results clearly demonstrate that full-length *Mtb*-ribA2 is required for optimal DHBPS activity. Previously, we have shown that *Mtb*-DHBPS can exist as an inactive monomer at pH 4.0 and as a functional dimer between pH 6.0 and 9.0 (in the absence of salt) in both the crystal structure as well as in solution (Singh *et al.*, 2011). The monomer of *Mtb*-DHBPS obtained at pH 4.0 is catalytically inactive as it undergoes a conformational change in loop3 in the vicinity of the active site that results in loss of activity (Singh *et al.*, 2011). However, the DHBPS domain of *Mtb*-ribA2 does not show such a conformational change, as revealed by the present crystal structure and as reported previously (Singh *et al.*, 2011). Nevertheless, the kinetic values for both the DHBPS and the GCHII domain of *Mtb*-ribA2 are substantially lower compared with other species in which these are expressed as separate proteins. Similarly low catalytic activities have also been reported for ribA in the case of *A. thaliana* and tomato (Herz *et al.*, 2000). However, in the case of *B. subtilis* the catalytic activity of ribA is comparable with that in species in

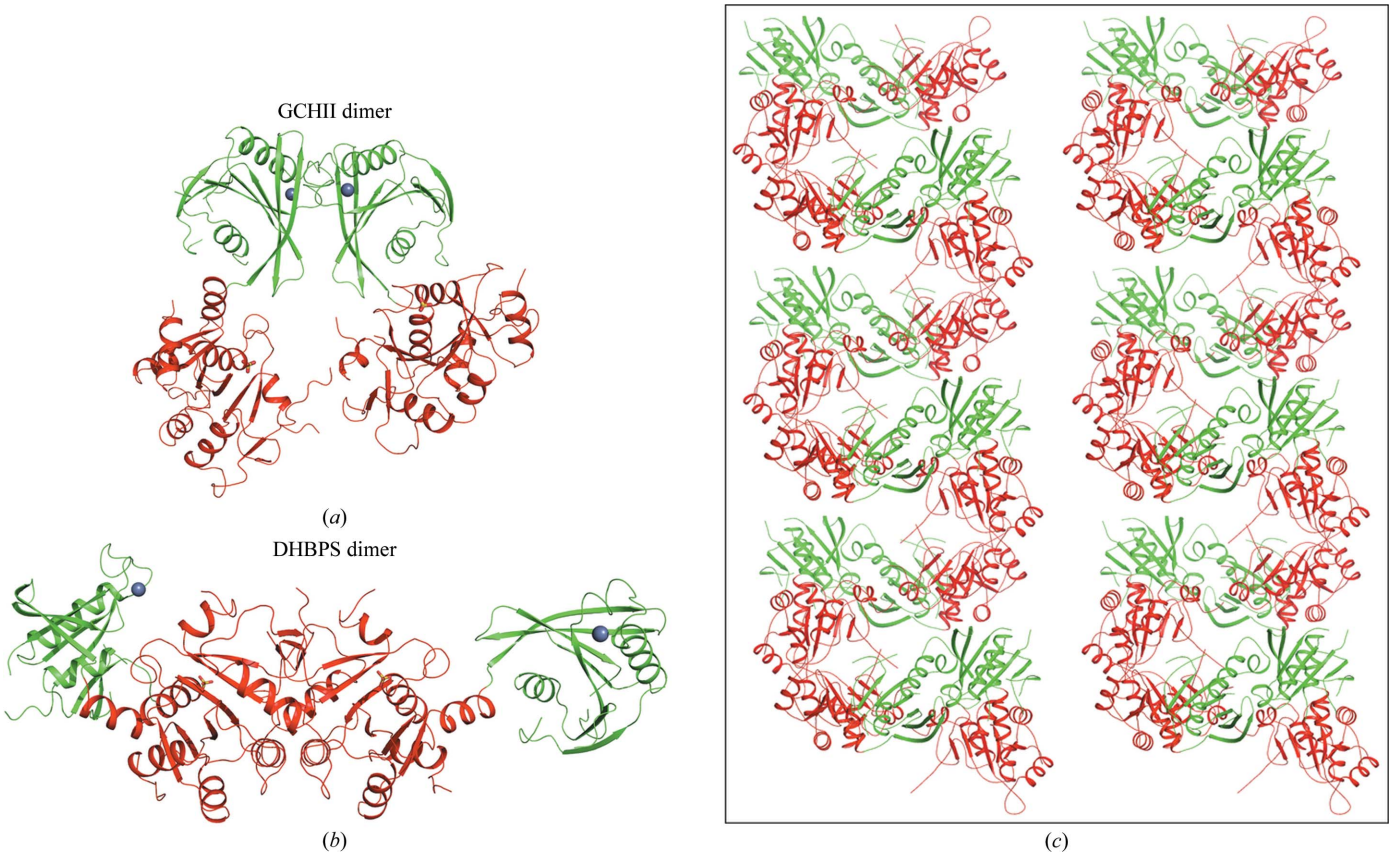

Figure 7
The alternate possible arrangements of *Mtb*-ribA2 molecules in the asymmetric unit: (*a*) with GCHII as a dimer, (*b*) with DHBPS as a dimer. (*c*) Crystal packing shows a long 'helical-like' structure formed by both the GCHII dimer (green) and the DHBPS dimer (red) of *Mtb*-ribA2.

which they are encoded as separate proteins (Hümbelin *et al.*, 1999; Lehmann *et al.*, 2009). While differences between the amino-acid sequences among these species may contribute to the enzyme activity, further studies are required to understand the poor activity shown by the DHBPS and GCHII domains of *Mtb*-ribA2.

4. Conclusions

In *Mtb*, the *ribA1* and *ribA2* genes are predicted to encode bifunctional DHBPS/GCHII enzymes. While *ribA2* has been shown to be essential for the growth of *Mtb* (Sassetti *et al.*, 2003; Griffin *et al.*, 2011), *ribA1* was found to be a non-essential gene (Sassetti *et al.*, 2003). The presence of multiple copies of the *ribA*, *ribB* and *ribBA* genes coding for GCHII, DHBPS and bifunctional DHBPS/GCHII, respectively, in bacterial genomes has been reported previously and has been suggested to play a role in certain stressful conditions and in acquiring functional divergence using the same enzyme scaffold (Knegt *et al.*, 2008; Spoonamore & Bandarian, 2008). The crystal structures and molecular mechanisms of GCHII and DHBPS are known for cases in which these enzymes are encoded as separate genes. However, their organization and molecular mechanism as a bifunctional enzyme is still elusive. Here, we report the crystal structure of the first bifunctional ribA2 enzyme from *Mtb*, which is shown to be essential for this pathogen. Our studies demonstrate that *Mtb*-ribA2 forms a dimer in solution through its GCHII domains and shows both GCHII and DHBPS catalytic activities. While the GCHII domain of *Mtb*-ribA2 (*Mtb*-GCHII) is independently active, the DHBPS domain of *Mtb*-ribA2 shows poor catalytic activity, indicating that full-length *Mtb*-ribA2 is required for optimal DHBPS activity. In cases where DHBPS is expressed as a separate polypeptide chain it always exists as a dimer formed through hydrophobic interactions and the catalytic sites are formed at the dimeric interface. However, in the case of the bifunctional DHBPS/GCHII enzyme the DHBPS domain exists as a monomer and shows catalytic activity. Although experiments are required to understand the catalytic activity of DHBPS as a monomer, it is tempting to predict that the DHBPS may form a dimer transiently and catalyze the formation of DHBP as the active site is formed at the dimeric interface of the DHBPS domain (Singh *et al.*, 2011). In addition, while the physiological significance of the evolution of this bifunctional enzyme needs to be explored, we speculate that it may play a role in the regulation of riboflavin synthesis, as the DHBPS/GCHII enzymes have been shown to be rate-limiting enzymes in the riboflavin pathway (Hümbelin *et al.*, 1999). Riboflavin is the sole precursor for the synthesis of FMN and FAD, which are essential cofactors for many cellular enzymes. Thus, the regulation of gene expression of two rate-limiting enzymes by a single promoter will have a greater advantage during stress as it can regulate both rate-limiting enzymes to synthesise riboflavin according to need. Nevertheless, the structure determined in this report may provide a platform for identifying new drugs, as this enzyme is known to be a potential drug target for *Mtb*.

We thank Ms Sharanjit Kaur for help in carrying out the MALDI analysis. MS, PK, SY, RG and NS acknowledge the Council of Scientific and Industrial Research (CSIR), Government of India for their doctoral fellowships. We also thank Dr Balvinder Singh for carefully reading the manuscript. This work was supported by CSIR through network project SIP10.

References

Bacher, A. (1991). *Chemistry and Biochemistry of Flavoenzymes*, edited by F. Müller, pp. 349–370. Boca Raton: CRC Press.
Bacher, A., Richter, G., Ritz, H., Eberhardt, S., Fischer, M. & Krieger, C. (1997). *Methods Enzymol.* **280**, 382–389.
Bradford, M. M. (1976). *Anal. Biochem.* **72**, 248–254.
Brünger, A. T. (1992). *Nature (London)*, **355**, 472–475.
Burrows, R. B. & Brown, G. M. (1978). *J. Bacteriol.* **136**, 657–667.
Campanella, J. J., Bitincka, L. & Smalley, J. (2003). *BMC Bioinformatics*, **4**, 29.
Cole, S. T. *et al.* (2001). *Nature (London)*, **409**, 1007–1011.
Echt, S., Bauer, S., Steinbacher, S., Huber, R., Bacher, A. & Fischer, M. (2004). *J. Mol. Biol.* **341**, 1085–1096.
Emsley, P., Lohkamp, B., Scott, W. G. & Cowtan, K. (2010). *Acta Cryst.* D**66**, 486–501.
Fassbinder, F., Kist, M. & Bereswill, S. (2000). *FEMS Microbiol. Lett.* **191**, 191–197.
Fischer, M. & Bacher, A. (2008). *Arch. Biochem. Biophys.* **474**, 252–265.
Foor, F. & Brown, G. M. (1975). *J. Biol. Chem.* **250**, 3545–3551.
Foor, F. & Brown, G. M. (1980). *Methods Enzymol.* **66**, 303–307.
French, S. & Wilson, K. (1978). *Acta Cryst.* A**34**, 517–525.
Gerdes, S. Y. *et al.* (2001). *J. Bacteriol.* **184**, 4555–4572.
Gouet, P., Courcelle, E., Stuart, D. I. & Métoz, F. (1999). *Bioinformatics*, **15**, 305–308.
Griffin, J. E., Gawronski, J. D., Dejesus, M. A., Ioerger, T. R., Akerley, B. J. & Sassetti, C. M. (2011). *PLoS Pathog.* **7**, e1002251.
Hayward, S. & Berendsen, H. J. (1998). *Proteins*, **30**, 144–154.
Herz, S., Eberhardt, S. & Bacher, A. (2000). *Phytochemistry*, **53**, 723–731.
Hümbelin, M., Griesser, V., Keller, T., Schurter, W., Haiker, M., Hohmann, H.-P., Ritz, H., Richter, G., Bacher, A. & van Loon, A. P. G. M. (1999). *J. Ind. Microbiol. Biotechnol.* **22**, 1–7.
Kabsch, W. (2010). *Acta Cryst.* D**66**, 125–132.
Kaiser, J., Schramek, N., Eberhardt, S., Püttmer, S., Schuster, M. & Bacher, A. (2002). *Eur. J. Biochem.* **269**, 5264–5270.
Katoh, K. & Toh, H. (2008). *Brief. Bioinform.* **9**, 286–298.
Kelly, M. J., Ball, L. J., Krieger, C., Yu, Y., Fischer, M., Schiffmann, S., Schmieder, P., Kühne, R., Bermel, W., Bacher, A., Richter, G. & Oschkinat, H. (2001). *Proc. Natl Acad. Sci. USA*, **98**, 13025–13030.
Kis, K. & Bacher, A. (1995). *J. Biol. Chem.* **270**, 16788–16795.
Kis, K., Volk, R. & Bacher, A. (1995). *Biochemistry*, **34**, 2883–2892.
Kleywegt, G. J. (1996). *Acta Cryst.* D**52**, 842–857.
Knegt, F. H., Mello, L. V., Reis, F. C., Santos, M. T., Vicentini, R., Ferraz, L. F. & Ottoboni, L. M. (2008). *Res. Microbiol.* **159**, 423–431.
Krissinel, E. & Henrick, K. (2004). *Acta Cryst.* D**60**, 2256–2268.
Krissinel, E. & Henrick, K. (2007). *J. Mol. Biol.* **372**, 774–797.
Kumar, P., Singh, M., Gautam, R. & Karthikeyan, S. (2010). *Proteins*, **78**, 3292–3303.
Laemmli, U. K. (1970). *Nature (London)*, **227**, 680–685.
Laskowski, R. A., MacArthur, M. W., Moss, D. S. & Thornton, J. M. (1993). *J. Appl. Cryst.* **26**, 283–291.
Lehmann, M., Degen, S., Hohmann, H. P., Wyss, M., Bacher, A. & Schramek, N. (2009). *FEBS J.* **276**, 4119–4129.
Liao, D.-I., Calabrese, J. C., Wawrzak, Z., Viitanen, P. V. & Jordan, D. B. (2001). *Structure*, **9**, 11–18.

Liao, D.-I., Zheng, Y.-J., Viitanen, P. V. & Jordan, D. B. (2002). *Biochemistry*, **41**, 1795–1806.
Long, Q., Ji, L., Wang, H. & Xie, J. (2010). *Chem. Biol. Drug Des.* **75**, 339–347.
Matthews, B. W. (1968). *J. Mol. Biol.* **33**, 491–497.
McCoy, A. J., Grosse-Kunstleve, R. W., Adams, P. D., Winn, M. D., Storoni, L. C. & Read, R. J. (2007). *J. Appl. Cryst.* **40**, 658–674.
Murshudov, G. N., Skubák, P., Lebedev, A. A., Pannu, N. S., Steiner, R. A., Nicholls, R. A., Winn, M. D., Long, F. & Vagin, A. A. (2011). *Acta Cryst.* D**67**, 355–367.
Painter, J. & Merritt, E. A. (2006). *Acta Cryst.* D**62**, 439–450.
Picollelli, M. A., Viitanen, P. V. & Jordan, D. B. (2000). *Anal. Biochem.* **287**, 347–349.
Plaut, G. W. (1960). *J. Biol. Chem.* **235**, 41–42.
Plaut, G. W. (1963). *J. Biol. Chem.* **238**, 2225–2233.
Plaut, G. W., Beach, R. L. & Aogaichi, T. (1970). *Biochemistry*, **9**, 771–785.
Ren, J., Kotaka, M., Lockyer, M., Lamb, H. K., Hawkins, A. R. & Stammers, D. K. (2005). *J. Biol. Chem.* **280**, 36912–36919.
Richter, G., Fischer, M., Krieger, C., Eberhardt, S., Lüttgen, H., Gerstenschläger, I. & Bacher, A. (1997). *J. Bacteriol.* **179**, 2022–2028.
Richter, G., Ritz, H., Katzenmeier, G., Volk, R., Kohnle, A., Lottspeich, F., Allendorf, D. & Bacher, A. (1993). *J. Bacteriol.* **175**, 4045–4051.
Richter, G., Volk, R., Krieger, C., Lahm, H. W., Röthlisberger, U. & Bacher, A. (1992). *J. Bacteriol.* **174**, 4050–4056.
Russell, D. G., Barry, C. E. III & Flynn, J. L. (2010). *Science*, **328**, 852–856.
Sassetti, C. M., Boyd, D. H. & Rubin, E. J. (2003). *Mol. Microbiol.* **48**, 77–84.
Singh, M., Kumar, P. & Karthikeyan, S. (2011). *J. Struct. Biol.* **174**, 374–384.
Spoonamore, J. E. & Bandarian, V. (2008). *Biochemistry*, **47**, 2592–2600.
Spoonamore, J. E., Dahlgran, A. L., Jacobsen, N. E. & Bandarian, V. (2006). *Biochemistry*, **45**, 12144–12155.
Steinbacher, S., Schiffmann, S., Richter, G., Huber, R., Bacher, A. & Fischer, M. (2003). *J. Biol. Chem.* **278**, 42256–42265.
Teng, T.-Y. (1990). *J. Appl. Cryst.* **23**, 387–391.
Volk, R. & Bacher, A. (1990). *J. Biol. Chem.* **265**, 19479–19485.
Volk, R. & Bacher, A. (1991). *J. Biol. Chem.* **266**, 20610–20618.
Winn, M. D. *et al.* (2011). *Acta Cryst.* D**67**, 235–242.
World Health Organization (2012). *Global Tuberculosis Report 2012*. Geneva: World Health Organization. http://www.who.int/tb/publications/global_report/en/.